

## **DEVELOPMENT AND ANALYSIS OF FLEXIBLE UHF RFID ANTENNAS FOR “GREEN” ELECTRONICS**

**Y. Amin\***, **Q. Chen**, **L.-R. Zheng**, and **H. Tenhunen**

iPack VINN Excellence Center, Royal Institute of Technology (KTH), Stockholm SE-16440, Sweden

**Abstract**—In this paper, novel Bowtie antennas which cover complete UHF RFID band (860–960 MHz), fabricated on various ultra-low-cost substrates using state-of-the-art printing technologies are investigated as an approach that aims to accommodate the antenna during the package printing process whilst faster production on commercially available paper. The proposed antenna structures are evaluated in reference to circuit and field concepts, to exhibit extreme degree of functional versatility. These antennas are developed to cater the variations which appear in electromagnetic properties and thickness of paper substrate due to various environmental effects. Computed (simulated) and well-agreed measurement results confirm a superior performance of the tag modules while stepping towards next generation of “green” tags.

### **1. INTRODUCTION**

In recent years, the recognition of radio frequency identification (RFID) technology has greater than before and comprehensively integrated into modern society applications, ranging from remote monitoring sensing to more demanding operational conditions in logistics, healthcare and access control [1–4]. Ultra-High frequency (UHF) RF identification (RFID) systems employing modulated backscatter communication links, such as those based on the widely deployed ISO18000-6c or EPC Global Class 1 Generation 2 specification [5], have traditionally been analyzed using techniques first developed to analyze radar systems. Compared to conventional identification method or barcodes, RFID technology offers several advantages, such as the ability for simultaneously reading a number of tags, higher reading range, and faster data transfer [6].

---

*Received 6 June 2012, Accepted 9 July 2012, Scheduled 13 July 2012*

\* Corresponding author: Yasar Amin (ysar@kth.se).

Passive RFID tags do not have any internal source of energy, such as a battery, to support the functioning. Passive tags get all the energy needed for functioning from the electromagnetic radiation emitted by the reader. Communication between the reader and the tag is based on backscattering principle in which reader transmits energy to activate the tag, and then the tag responds by backscattering its identification information to the reader. In general, an RFID tag consists of an antenna and an application-specific integrated circuit chip (strap or RFIC). For low-cost and reliable production of RFID tags, the fabrication methods and materials for antennas are considered to be challenges [7–9]. Moreover, the research area appears deserted while addressing the new rising issues interrelated to the field of economic and eco-friendly tags comprising of paper substrate [10, 11]. Paper substrates offer numerous advantages for manufacturing RFID tags, not only is paper extensively available, and inexpensive it is lightweight, recyclable and can be rolled or folded into 3D configurations [12, 13].

This paper presents a thorough analysis of novel rounded-corner bowtie passive RFID tag antennas, which are fabricated on various ultra-low-cost substrates (characterized & evaluated for the proposed antenna in Table 1 in combination with the state-of-the-art printing technologies (Screen Printing, Rotary Printing (Flexo), Inkjet printing & (Dry Phase Patterning) mentioned in Table 2. The implementation of T-match arms for matching of the antenna to the integrated circuit (IC) is introduced that improves the reliability against environmental diversities as well as increase the maximum reading distance. The design and simulations are performed using ANSYS HFSS<sup>TM</sup> whereas; the measurements are carried out in an anechoic chamber along with the reader setup dedicated to antenna characterization. The proposed antenna operates from 860–960 MHz, thus expands to the

**Table 1.** Characterized/evaluated substrate parameters.

Substrate	Thickness ( $\mu\text{m}$ )/ Permittivity ( $\epsilon_r$ )/Loss Tangent	Applications
Kodak U-P Photopaper	250/3.3 (avg.)/0.077 (1 GHz@25°)	Packaging
HP Adv. Photopaper	250/3.3 (avg.)/0.04 (1 GHz@25°)	Packaging
Paper (p_e:smart)	250/3.2 (avg.)/0.077 (1 GHz@25°)	Packaging
Paper (Korsnäs)	375/3.3 (avg.)/0.077 (1 GHz@25°)	Packaging
Teonex Q51	25/2.9/0.005 (1 GHz@25°)	Harsh environment
Kapton HN	125/3.5/0.0026 (1 kHz@25°)	Harsh environment
Metal coated PET	50/3.3/0.003 (0.9 GHz@25°)	Fully wrapable

**Table 2.** Printing technology/ink/substrate/speed combinations.

Inkjet Printing	Rotary Printing	Screen Printing	DPP
<i>Cabot Ink</i>	<i>Asahi</i>	<i>Asahi</i>	<i>Al Coated</i>
<i>CCI-300</i>	<i>Paste (LS-411AW)</i>	<i>Paste (LS-411AW)</i>	
Kodak Photopaper	Kapton HN	Kapton HN	PET
HP Photopaper	Teonex Q51 (2 & 4 m/min)	Paper (Korsnäs)	
Paper (p_e:smart)	Paper (Korsnäs)		

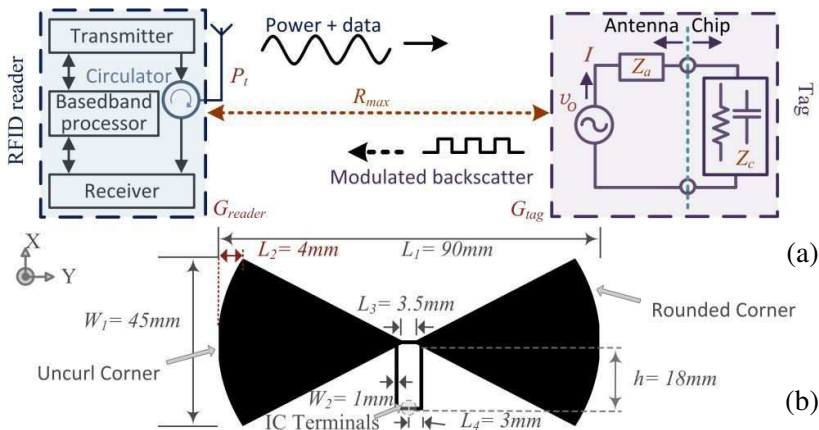


**Figure 1.** (a) Far-field RFID mechanism & equivalent circuit of an IC tag, (b) T-match folded rounded-corner bowtie RFID tag module configuration.

global usage of this tag. The robustness, eco-friendliness, flexibility and outstandingly read range of the proposed antennas make them an absolute choice for far-field industrial applications (a few mentioned in Table 1).

## 2. ANTENNA DIMENSIONS AND PARAMETRIC OPTIMIZATION

The main purpose of optimization is to maximize the feeding power to the load to achieve the maximum possible read range while preserving the multifaceted nature of the proposed antenna. The NXP ucode g2xm (SOT1040AB2 (Al strap), e.g., the target IC impedance at 915 MHz is  $13.3 - j122 \Omega$ ) is selected. Figure 1(a) shows the Thevenin equivalent circuit of the IC tag, from which we can calculate the

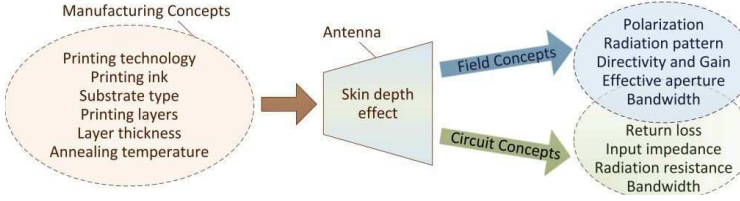


**Figure 2.** An outline of key antenna development parameters.

key design criteria. Antenna input impedance  $Z_a$  is expressed as the impedance offered by an antenna at its terminals or the ratio of the voltage to current at its terminals. Mathematically, it is calculated as:

$$Z_a = \frac{v_o}{I} = R_a + jX_a \quad (1)$$

where  $v_o$  is the input voltage and  $I$  the current at the antenna input. The input impedance is a complex number, and the real part further consists of two components. So, it is worth mentioning here that throughout the text onwards whenever input impedance of antenna is referred it will be meant that the real part  $R_a$  of the antenna input impedance  $Z_a$  consists of the radiation resistance and the antenna losses or loss resistance.

The proposed antenna structure is shown in Figure 1(b) along with dimensions and IC terminals placed in the center of the T-match arms. The T-match arms are also responsible for the matching of the antenna impedance to that of the IC through the fine tuning of the length  $L_4$ , height  $h$ , and width  $W_2$ . In the proposed tag, antenna is directly connected to a source (IC or strap) of impedance  $Z_c = R_c + jX_c$ , for a matched load the following condition should be met:

$$Z_c = Z_a^* = R_a - jX_a \quad (2)$$

Thus, the impedance matching between  $Z_a$  and  $Z_c$  will stand for the optimal antenna. This ultimate goal defines the essence of antenna design in order to control the current distribution, which in turn determines the radiation pattern and input impedance. Therefore, to assess development process thoroughly all relevant parameters of antenna are analysed here, which are categorized from the manufacturing, circuit and field point of views as summarized in Figure 2.

### 2.1. Antenna Effective Aperture and Aperture Efficiency

In the proposed antenna, conscientious effort has been carried out to optimize antenna dimensions. Since the field/current, on the antenna

aperture is not uniform, the concept of antenna effective aperture is established. In achieving high performance while keeping the minimum antenna size, an established concept that the effective aperture  $A_e$  is less than the physical aperture  $A_p$  is accomplished [14]. Thus, the aperture efficiency is mathematically expressed as the ratio of these two terms. For a good antenna structure, this parameter should be in the range of 50–80%. The effective aperture is proportional to the directivity of the antenna, and the directivity can also be expressed in terms of the aperture size and aperture efficiency:

$$D = \frac{4\pi}{\lambda^2} A_e = \frac{4\pi}{\lambda^2} \eta_{ap} A_p \quad (3)$$

By knowing the power density  $S$  at the receiving antenna, we can estimate the received power by using the following equation:

$$P_r = S A_e \quad (4)$$

This optimization parameter enriched the key design criteria to save every drop of the manufacturing ink and material in order to make low-cost as well as environmental friendly tags.

## 2.2. Skin Depth Effect and Antenna Performance

The skin depth and ohmic losses of the printed conductive layer set the boundary conditions for the printing technologies, and parameters such as the amount of silver ink depending upon its conductivity and the thickness of the printed layers. Mathematically, the skin depth is, therefore, expressed as:

$$\text{FieldConcept} \rightarrow \left( \delta \approx \sqrt{\frac{1}{\pi f \mu \sigma}} \right) = \text{CircuitConcept} \rightarrow \left( J = J_0 e^{-z/\delta} \right) \quad (5)$$

and from circuit concept it is defined as the depth below the surface of the conductor at which the current density decays to  $1/e$  (about 37%) of the current density at the surface [14]. Equation (5) leads to the manufacturing parameters of the proposed antenna mentioned in Figure 2. In a good conductor, skin depth varies as the inverse square root of the conductivity. Thus, better conductors have a reduced skin depth, and this factor plays a key role in investigating optimal printing techniques for fabrication.

## 3. MANUFACTURING PARAMETRIC ANALYSIS

The manufacturing processes are analyzed primarily with a focus on low cost solutions available for industrial applications at present. In general, the comparison of the exact cost for each printing process

depend upon the number of factors which make such analysis out of scope of this article. However, relative comparison of cost per tag is carried out while implementing each technology and on the basis of this study each fabrication technology is given the scale value from (1) to (4), where (4) corresponds to the cheapest solution.

### 3.1. Screen Printing — (2)

One of the recent areas, where screen has made itself welcome is in the printing of RFID antennas. The technological advancements have made it possible to print antennas through the process of screen printing, by using conventional substrates or materials.

The proposed antennas are screen printed with the semiautomatic screen printer (Figure 3(a)) in VTT (Technical Research Centre of Finland) on Kapton HN and Korsnäs paper, as showed in Figures 3(b) & (c), respectively. The 25  $\mu\text{m}$  thick layer is printed using Asahi paste in order to exploit its outstanding mechanical performance [15], while remarkably stable ink distribution all over the printed patterns is achieved. Robust proposed RFID tag antennas are achieved by this process, which can maintain their performance even being bent several times, this is demonstrated with detail in [16]. The characterization and measurements of the printed traces are carried out using Veeco profilometer, which are presented in Figures 3(d)–(f). The samples are post-annealed for 2 hours at 140°C to achieve improved conductivity.

### 3.2. Rotary Printing — (4)

Rotary printing, is a finer resolution printing (flexo) technology, it is rapidly gaining importance by RFID antenna printing providers as a manufacturing choice that offers higher throughput than screen printing.

The rotary screen printing of antennas is studied here using VTT's ROKO pilot line showed in Figure 4(a). PEN, polyimide and paper substrates are used with two silver PTF — (Polymer Thick Film) inks and one silver nanoparticle ink. Additionally, the printing screen mesh size is varied in these test runs to study its effects on, e.g., layer thickness. A hot air drying oven having length of 4 m is used. The performance of rotary printed antennas showed in Figures 4(b)–(d) depend on several parameters. The line thickness is typically 10–15  $\mu\text{m}$ , and sheet resistance 50  $\text{m}\Omega/\text{square}$ , which can be further decreased to 30  $\text{m}\Omega/\text{square}$  by additional oven drying. The best print quality is obtained using a printing speed of 2 m/min.

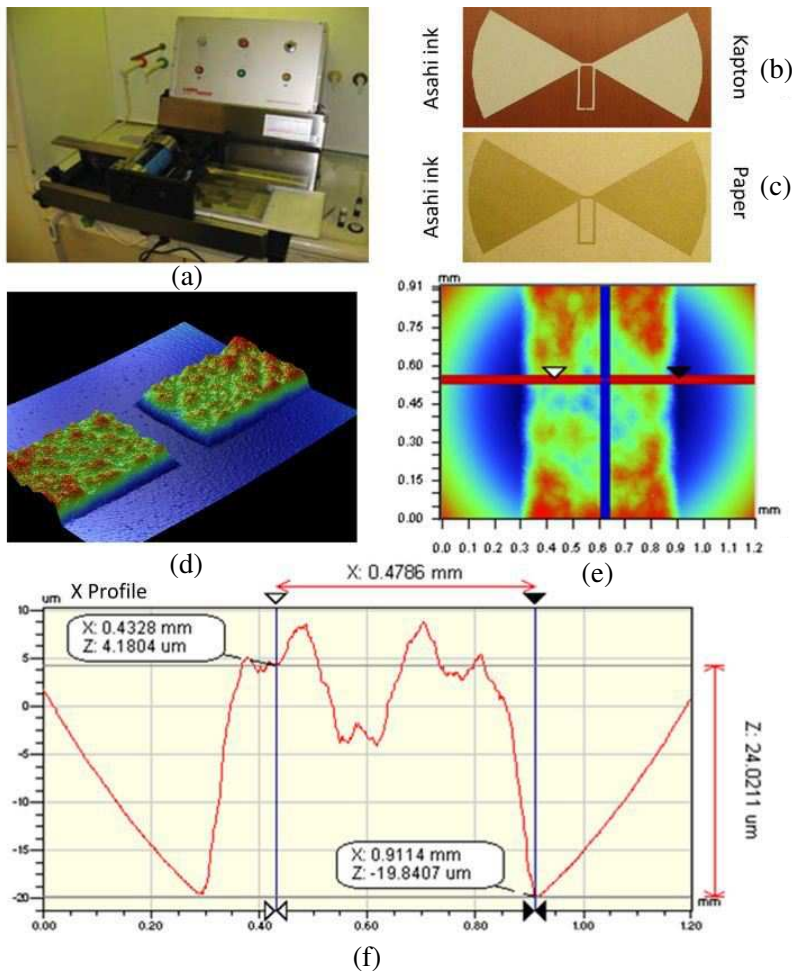


**Figure 3.** (a) Screen printing setup; Screen printed antenna on: (b) Kapton HN, (c) Korsnäs paper; Profilometer measurement of printed layer: (d) roughness, (e) surface topography, (f) thickness.

### 3.3. Dry Phase Patterning — (3)

The Proposed antennas are also developed using Dry Phase Patterning (DPP) for comparison and validation of the concept (in Acreo AB, Sweden), a method for patterning metal layers on flexible substrates. The laminate of Aluminum/PET is patterned for proposed antennas showed in Figure 5(c). Process speed up to 150 m/min and line pitch down to 250  $\mu\text{m}$  has been demonstrated, which made DPP a better choice for cost effective RFID tags.

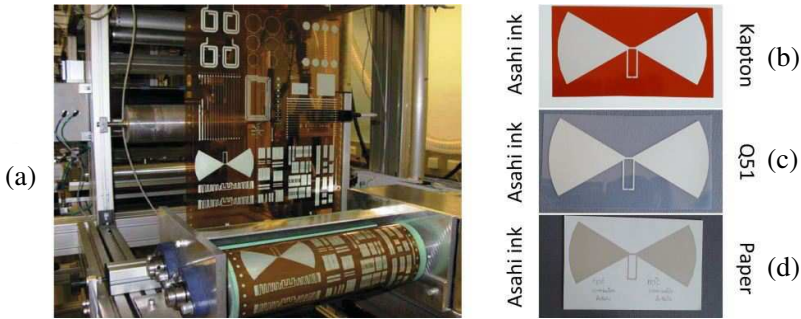


**Figure 4.** (a) Rotary printing setup; Rotary printed antenna on: (b) Kapton HN, (c) Q51, (d) Korsnäs paper.

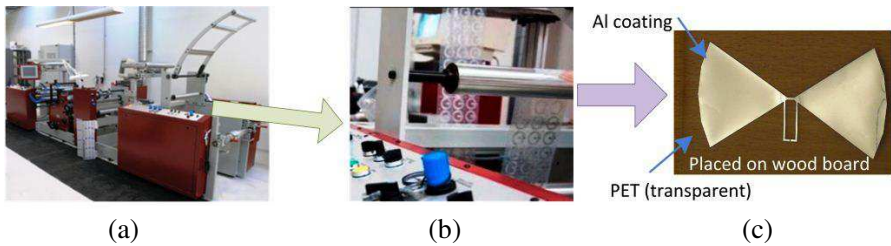


**Figure 5.** (a) DPP setup at Acreo, (b) antenna patterning, (c) aluminum patterned antenna on PET.

Laboratory production line showed in Figures 5(a) & (b) is used for the test trials. One of the main benefits of employing DPP method for the fabrication of proposed antennas is the reduced load on the environment which embraces the concept of “green” tags. This is mainly because of reduced energy consumption; no washing, brushing or drying is required. Since, no chemicals are used, the residual product is in a dry and easily recyclable form.

### 3.4. Inkjet Printing — (1)

Inkjet printing is a direct-write mechanism by which the desired design outline is transferred directly to the (flexible) substrate. This technology requires no masks compared with the conventional etching technique, which has been commonly used in industry. During inkjet printing, the single ink droplet is jetted from the nozzle to the desired position, therefore, creating no waste, ensuing in an economical and eco-friendly production choice.

The inkjet printing setup used in the present research is showed in Figure 6(a) and is based on a Fujifilm Dimatix DMP2800 printer. It uses one user fillable piezo-based inkjet print cartridge with 16 nozzles in a single row and  $254\ \mu\text{m}$  nozzle spacing, to eject 1 pl or 10 pl drops (depending upon the choice of cartridge). The printed structures on Kodak photopaper and (p.e:smart) from Felix Schoeller are showed in Figures 6(b) & (c), respectively. These are printed using 10 pL cartridge (DMC-11610) filled with Cabot conductive Ink (CCI-300 from Cabot Corp.), having viscosity of 11–15 cp, with silver solid loading of 19–21 wt% and density of 1.23–1.24 g/ml is jetted with printing resolution of 1270 dpi. The printing was carried out in a standard laboratory environment to determine the extent to which useable devices could be fabricated on a commercial scale printing method.

After the silver nanoparticle droplets are deposited to the substrate, the sintering process is carried out for 2 hr at  $150^\circ\text{C}$  for sufficiently curing, to remove the excess solvent and material impurities from the depositions. The characterization of the printed structures is carried out under ULTRA-55 Field Emission Scanning Electron Microscope from Carl Zeiss NTS showed in Figures 6(d) & (e). Figures 6(f) & (g) show the SEMs for elaborating the

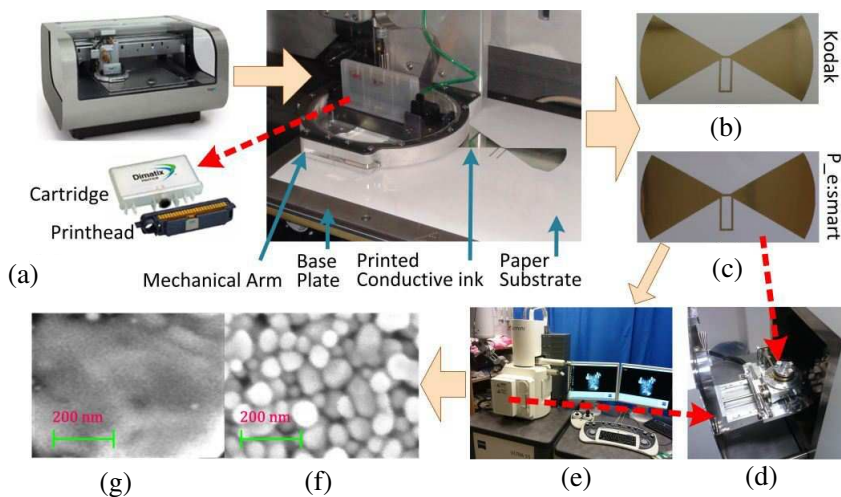


**Figure 6.** (a) Inkjet printing setup; Inkjet printed antenna on: (b) Kodak photopaper, (c) Felix Schoeller paper; (d) SEM sample holder, (e) ULTRA-55 FESEM Carl Zeiss setup; SEM images of three layers of printed silver nanoparticle ink, after curing 2 hr at: (f)  $100^\circ\text{C}$ , (g)  $150^\circ\text{C}$ .

difference between the heating temperature after a 2hr curing at 100°C and 150°C respectively. At high temperature, an almost solid metal conductor is formed so providing a percolation channel for the conduction of electrons throughout the material without obstruction. The sintering process also presents the derived benefit of increasing the bonding of the deposition with the paper substrate.

#### 4. FIELD & CIRCUIT CONCEPTS PARAMETRIC ANALYSIS

During the printing process of the proposed antennas, attention is given to fabricate five identical structures with the same combination of printing material, ambient conditions & technology. These prototypes are then measured across the UHF frequency band using half mirror method. Half mirror method is adapted instead of balun usage to eliminate the possibility of error [17]. Furthermore, maximum deviated data value at a frequency among five prototypes is reported here, which provides an in-depth view for the worst case analysis. Moreover, this technique provides the thorough investigation of reliability parameters for each printing technology.

Figures 7(a) & (b) show the impedance plots. Impedance measurements are taken using vector network analyzer (MS2026B, Anritsu). The standard calibration method short-open-load (SOL) is used. As showed in Figure 7(a), the computed resistance for the antenna in the UHF RFID frequency range maintains a value close to  $14\Omega$  between the two successive peaks. There is extremely small variation observed among the curves for different antennas, and it can be well illustrated from the Figure 7(a), that all the prototype antennas have maintained the resistance around  $14\Omega$  in a linear fashion with frequency. The reactance part of the impedance, as showed in Figure 7(b), follows a positive value with a linear variation with frequency, pertaining to an inductance that conjugately matches or, equivalently, cancels the effect of the  $1.42\text{ pF}$  input capacitance (parallel) of the IC. It is observed that a relatively constant concurrence is found between the computed and measured results.

The RFID IC/strap is attached to the IC terminals on printed structures with CW2400 silver conductive epoxy, cured at 24°C for 4 hours or 70°C for 10 minutes to achieve maximum conductivity and adhesion. The reading range of the proposed antenna is measured in response to Impinj's UHF RFID kit and reader antennas in an anechoic chamber, to validate the feasibility for commercial RFID system. The computations are carried out in accordance with the following Friis

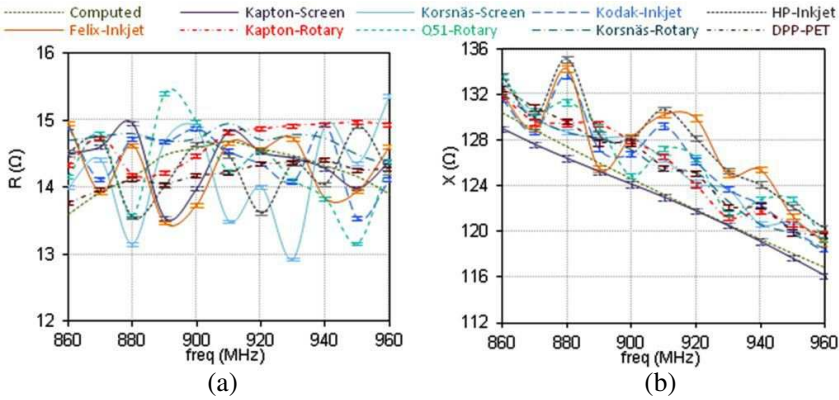


**Figure 7.** Antenna input: (a) resistance variation, (b) reactance variation.

equation:

$$R_{\max} = \sqrt[4]{\frac{P_t G_{tag}^2 G_{reader}^2 p^2}{P_{system}} \left(\frac{\lambda}{4\pi}\right)^4} \quad (6)$$

where the output power of the reader is  $P_t$ ,  $p$  the polarization efficiency,  $G_{tag}$  the realized gain of the tag antenna (including the mismatch between the tag antenna and the tag chip),  $G_{reader}$  the gain of the reader antenna,  $\lambda$  the wavelength in free space at the operating frequency, and  $P_{system}$  the sensitivity of the reader system in detecting the backscattered signal from the tag. It is observed that the read range can be influenced by the reader antenna in use. The measured and computed results are in close agreement, and the maximum read range achieved is 9 meters. The complete comparison of read range of different printed antennas is analysed in Figure 8(a), which exhibits the improved performance than previously published results [6, 18].

However, the read range is also susceptible to the tag orientation, the object which the tag is attached to, path loss, spatial and temporal fading statistics of the propagation environment [19]. In most UHF RFID systems, the reading distance obtained by Equation (6) extends well into the far-field region. When there is realization of tag which can operate in the far-field also involves near-field tag scanning. It can be projected that, in almost all cases, the tag gets more than sufficient power to operate when brought closer to RFID reader antenna. Hence, the read range of most UHF RFID tags is determined by the tag operational in the far-field [20].

The return loss of the antenna structure is calculated based on the power reflection coefficient. The computed return loss is showed

along with measured values of the rotary, screen, DPP & inkjet printed antennas in Figure 8(b). On the whole, a good agreement among the computed, and the manufactured antennas is pragmatic despite the higher metal loss of the silver-based conductive ink. Moreover, it is deduced from Figures 8(a) & (b) that the proposed antenna design can gracefully cater the variations in the properties of different substrates mentioned in Table 1. The characteristics of the bowtie profile of the half-wavelength dipole antenna body allows for a broadband operation. The bandwidth of the proposed antenna is 197 MHz, corresponding to 23% around the center frequency 855 MHz; so it covers the worldwide UHF RFID bands and can cater greater degree of environmental disparities. Furthermore, each calculation at a frequency is carried out by considering the variation of the IC reactance, which varies from  $130\text{--}116\ \Omega$  from  $850\text{--}960$  MHz, respectively. In general, it is sufficient by conjugately matching the antenna input impedance to those provided in the IC specifications by the manufacturer around the center frequency.

The radiation pattern is measured inside an anechoic chamber setup that replicates absolute free space, which is presented in Figure 9(a). The antenna under test (AUT) is mounted over the positioner assembly in the center of the chamber which is set to rotate the antenna in small steps of 5 degrees to obtain a  $360^\circ$  radiation pattern. A continuous-wave (CW) signal from the signal generator excites the AUT. The receiver antenna is connected to the spectrum analyzer (Agilent HP 8562E) and a PC running the test automation software controls the measurement setup. The normalized computed radiation pattern and the microwave chamber measurements

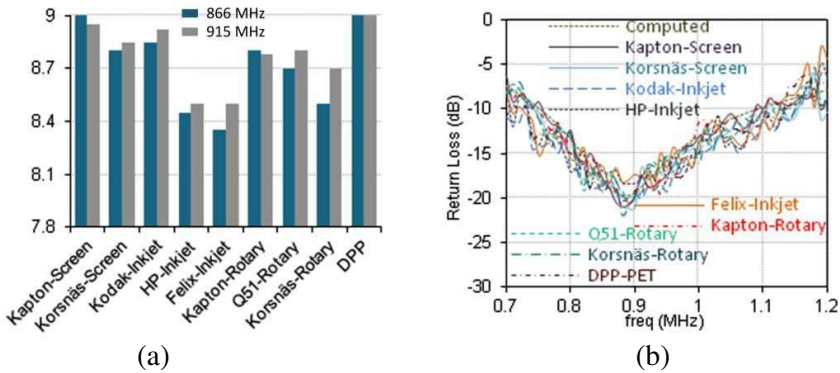


**Figure 8.** (a) Measured read range, (b) measured and computed return loss.

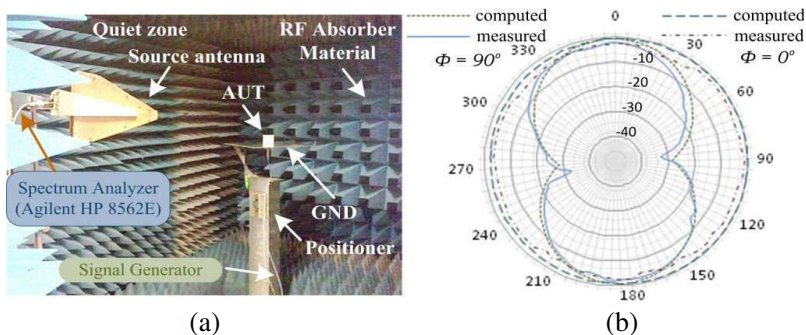


**Figure 9.** (a) The anechoic chamber setup, (b) measured & computed 2D far-field radiation plots.

are plotted in Figure 9(b). The radiation patterns are nearly uniform (omnidirectional) at 915 MHz with directivity around 2.1 dBi and show extreme agreement between computations and measurements, which can also be verified for other frequencies within the antenna bandwidth and are in coherence with previously published results [3, 6]. However, some distortion in the measurements is possibly due to the metal-plate structure [21], used for half mirror method which can be reduced by metal-plate fixture with curved edges [19].

## 5. CONCLUSION

In this paper, we introduced an innovative tag antenna capable of significantly increasing RFID reading range while being used on several substrates with different printing technologies. The proposed antenna has optimized effective aperture consisting of curled and uncurled corners along with T-matching network. The measured impedance bandwidth wholly covers the UHF RFID band and is capable of exhibiting long reading range of up to 9 m from 860–960 MHz, which is measured with a commercial RFID system. Numerous design parameters are optimized using successive iterations to obtain a single design which can be manufactured by various combinations of fabrication technology, ink and substrate that are potential candidates for “green” electronics solutions.

## ACKNOWLEDGMENT

This work was financially supported by Vinnova (The Swedish Governmental Agency for Innovation Systems) through the Vinn Excellence centers program.

**REFERENCES**

1. Marrocco, G., L. Mattioni, and C. Calabrese, "Multiport sensor RFIDs for wireless passive sensing of objects-basic theory and early results," *IEEE Transactions on Antennas and Propagation*, Vol. 56, No. 8, 2691–2702, 2008.
2. Tiang, J.-J., M. T. Islam, N. Misran, and J. S. Mandeep, "Circular microstrip slot antenna for dual-frequency RFID application," *Progress In Electromagnetics Research*, Vol. 120, 499–512, 2011.
3. Chen, S.-L., S.-K. Kuo, and C.-T. Lin, "A metallic RFID tag design for steel-bar and wire-rod management application in the steel industry," *Progress In Electromagnetics Research*, Vol. 91, 195–212, 2009.
4. Zuo, Y., "Survivable RFID systems: Issues, challenges, and techniques," *IEEE Transactions on Systems, Man, and Cybernetics*, Vol. 40, No. 4, 406–418, 2010.
5. Thomas, S. J., E. Wheeler, J. Teizer, and M. S. Reynolds, "Quadrature amplitude modulated backscatter in passive and semipassive UHF RFID systems," *IEEE Transactions on Microwave Theory and Techniques*, Vol. 60, No. 4, 1175–1182, 2012.
6. Rida, A., L. Yang, R. Vyas, and M. M. Tentzeris, "Conductive inkjet-printed antennas on flexible low-cost paper-based substrates for RFID and WSN applications," *IEEE Antennas and Propagation Magazine*, Vol. 51, No. 3, 13–23, 2009.
7. Panda, J. R. and R. S. Kshetrimayum, "A printed 2.4 GHz/5.8 GHz dual-band monopole antenna with a protruding stub in the ground plane for WLAN and RFID applications," *Progress In Electromagnetics Research*, Vol. 117, 425–434, 2011.
8. Hsu, H.-T., F.-Y. Kuo, and C.-H. Chang, "Application of quasi log-periodic antenna for UHF passive RFID tag design featuring constant power transmission coefficient over broadband operation," *Journal of Electromagnetic Waves and Applications*, Vol. 24, Nos. 5–6, 575–586, 2010.
9. Jamlos, M. F., T. A. Rahman, M. R. Kamarudin, P. Saad, M. A. Shamsudin, and A. M. M. Dahlan, "A novel adaptive Wi-Fi system with RFID technology," *Progress In Electromagnetics Research*, Vol. 108, 417–432, 2010.
10. Alimenti, F., et al., "A new contactless assembly method for paper substrate antennas and UHF RFID chips," *IEEE Transactions on Microwave Theory and Techniques*, Vol. 59, No. 3, 627–637, 2011.
11. Lazaro, A., D. Girbau, and R. Villarino, "Effects of interferences

- in UHF RFID systems,” *Progress In Electromagnetics Research*, Vol. 98, 425–443, 2009.
12. Bose, I. and S. Yan, “The green potential of RFID projects: A case-based analysis,” *IEEE IT Pro.*, Vol. 13, No. 1, 41–47, 2011.
  13. Makimura, H., et al., “Evolutional design of small antennas for passive UHF-band RFID,” *IEEE Journals and Magazines*, Vol. 47, No. 5, 1510–1513, 2011.
  14. Huang, Y. and K. Boyle, *Antennas from Theory to Practice*, John Wiley & Sons Ltd., New York, 2008.
  15. Jaakola, T., et al., “Low cost printed flexible multilayer substrates,” *10th Electronics Packaging Technology Conference, EPTC 2008*, 344–349, 2008.
  16. Amin, Y., Q. Chen, H. Tenhunen, and L. R. Zheng, “Evolutionary versatile printable RFID antennas for “Green” electronics,” *Journal of Electromagnetic Waves and Applications*, Vol. 26, Nos. 2–3, 264–273, 2012.
  17. Leong, K. S., M. L. Ng, and P. H. Cole, “Investigation of RF cable effect on RFID tag antenna impedance measurement,” *IEEE Antennas and Propagation Society Int.’ Symposium*, 573–576, 2007.
  18. Bjorninen, T., A. Z. Elsherbeni, and L. Ukkonen, “Low-profile conformal UHF RFID tag antenna for integration with water bottles,” *IEEE Antennas and Wireless Propagation Letters*, Vol. 10, 1147–1150, 2011.
  19. Amin, Y., Q. Chen, H. Tenhunen, and L. R. Zheng, “Performance-optimized Quadrature bowtie RFID antennas for cost-effective and eco-friendly industrial applications,” *Progress In Electromagnetics Research*, Vol. 126, 49–64, 2012.
  20. Tikhov, Y., “Comments on ‘antenna design for UHF RFID tags: A review and a practical application’,” *IEEE Transactions on Antennas and Propagation*, Vol. 54, No. 6, 2006.
  21. Kuo, S.-K., S.-L. Chen, and C.-T. Lin, “An accurate method for impedance measurement of RFID tag antenna,” *Progress In Electromagnetics Research*, Vol. 83, 93–106, 2008.